THE JOURNAL OF PHYSICAL CHEMISTRY B

Article

pubs.acs.org/JPCB

Thermodynamics and Intrinsic Structure of the Al−Pb Liquid−Liquid Interface: A Molecular Dynamics Simulation Study

Yang Yang[†] and Brian B. Laird*[,‡]

[†]Department of Materials Science and Engineering, University of California, Berkeley, Berkeley, California 94720, United States

[‡]Department of Chemistry, University of Kansas, Lawrence, Kansas 66045, United States

ABSTRACT: We examine the thermodynamics and intrinsic structure of the Al−Pb liquid−liquid interface using molecular dynamics simulation and embedded atom method potentials. The instantaneous interfacial positions, from which the intrinsic structure and the capillary fluctuation spectrum are determined, are calculated using a grid-based method. The interfacial free energy extracted from the capillary fluctuation spectrum is shown to be in excellent agreement with that calculated mechanically by integrating the stress profile. The intrinsic liquid−liquid interfacial density profile shows structural oscillations in the liquid phases in the interfacial region that are shown to be quantitatively similar to the radial distribution functions of the bulk liquid, consistent with theoretical predictions from classical density functional theory and with earlier simulations on liquid−liquid and liquid−vapor interfaces. In addition, we show the mean interfacial density profile for this system is well described as a convolution of the intrinsic density profile and the probability distribution of interfacial position.

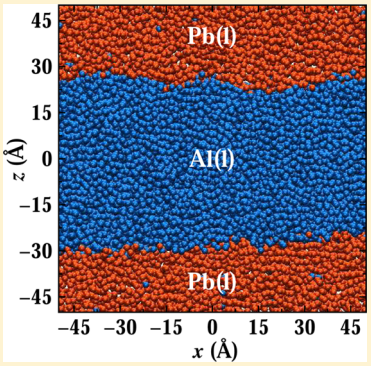

I. INTRODUCTION

Although not as extensively studied as solid−liquid or liquid−vapor interfaces, liquid−liquid interfaces can play a role in a number of technologically relevant fields, such as electrochemistry[1,2] or surfactant and nanoparticle assembly.[3,4] Liquid−liquid interfaces are similar to liquid−vapor interfaces in that the interfacial structure is broadened by capillary fluctuations,[5,6] making it difficult to resolve the intrinsic density profile that describes the local instantaneous interfacial structure.

Recent developments in molecular simulation methods, however, have made it possible to directly determine the intrinsic structure of fluid interfaces at the atomic/molecular level,[7−13] decoupling it from the capillary fluctuations. Most of these efforts have been focused on liquid−vapor interfaces,[7,11,14−22] and the few studies on liquid−liquid interfaces have examined interfaces between two immiscible molecular fluids, especially between water and organic liquids, such as hydrocarbons, dichloromethane, or CCl_4.[8,9,23−31] Studies involving atomic fluids have been limited to very highly idealized symmetric interfaces between immiscible Lennard-Jones (LJ) fluids.[32] Validating a prediction from classical density functional theory by Evans et al.,[33] these studies show that the intrinsic density profiles for liquid−vapor and liquid−liquid interfaces show structural density oscillations in the liquid near the interface that are quanitatively similar to the radial distribution functions of the bulk liquid phases.

In classical capillary wave theory (CWT), it is assumed that the mean interfacial equilibrium mean density profile, $\rho(z)$, which is the space and time average of the instantaneous inhomogeneous density, can be represented as a convolution of the intrinsic density profile, $\hat{\rho}(z)$, and the probability distribution of instantaneous interfacial position, $P_{\xi}(z)$,[34]

$$\rho(z) = \int \mathrm{d}z' \hat{\rho}(z - z')\, P_{\xi}(z') \tag{1}$$

In this picture, the local interfacial positions are assumed to be uncorrelated with the local intrinsic density profile and the capillary fluctuations rigidly shift the intrinsic profile according to the distribution $P_{\xi}(z)$. The convolution assumption offers a simple physical picture of how the intrinsic structure of the interface is broadened by capillary wave fluctuations. A recent study by Fernandez et al.[35] has reported a significant discrepancy between the mean density profile of a LJ liquid−vapor interface and the convolution of the measured intrinsic density profile and interface position probability distribution predicted from CWT. This discrepancy was interpreted to imply the breakdown of eq 1 due to correlation between the intrinsic profile and the position distribution. Chowdhary and Ladanyi[8] examined water/hydrocarbon liquid−liquid interfaces and showed qualitative, but not completely quantitative, agreement between the measured mean density profile and its prediction from eq 1 using a directly calculated position distribution. The examination of the validity of eq 1 is one of the motivations for this work.

In this work, we examine with molecular dynamics (MD) simulation, the intrinsic structure, and thermodynamics of a size-asymmetric liquid−liquid interface between liquid alumi-

Special Issue: James L. Skinner Festschrift

Received: February 24, 2014
Revised: March 28, 2014
Published: April 8, 2014

   dx.doi.org/10.1021/jp5019313 | J. Phys. Chem. B 2014, 118, 8373−8380

num (Al) and liquid lead (Pb). This system has a broad liquid−liquid miscibility gap above the melting point of Al (T_m^{Al}) and this study focuses on the system at T_m^{Al}, where the two fluids are nearly completely immiscible. This work is a complement to our previous study of solid−liquid interfaces in this system, in which we predicted the existence of solid−liquid premelting just below the Al melting temperature.[36] In this premelting transition, a film of liquid Al forms at the interface between the coexisting solid Al and liquid Pb phases, with a thickness that diverges as the temperature is increased to T_m^{Al}. One of the necessary quantities necessary to understand the thermodynamics of this premelting transition is the liquid−liquid interfacial free energy, γ_{ll}. Here we calculate γ_{ll} using both a mechanical approach, in which γ_{ll} is determined from the total excess stress of the interface,[37−39] and a method based on capillary fluctuations.[40] The capillary fluctuations are determined using an instantaneous interfacial position determined using the grid-based intrinsic profile (GIP) method of Jorge et al.[9,30] This calculation allows us also to determine both the intrinsic density profile and the probability distribution of interfacial position and to directly test the convolution assumption for this liquid−liquid interface.

II. SYSTEM AND SIMULATION DETAILS

The Al−Pb system, a typical monotectic model alloy that has a broad liquid−liquid miscibility gap, is modeled using the many-body EAM potential developed by Landa et al.[41] The melting points for Pb and Al, as well as the liquid-state miscibility gap, are well described by this potential.[36,42] The MD simulations reported here were carried out using the parallel MD code LAMMPS, distributed by Sandia National Laboratory.[43] Following the interfacial equilibration protocols reported in our previous studies of solid−liquid interfaces for this system,[36,42] well-equilibrated liquid−liquid interfaces were constructed at the melting temperature for Al for this model ($T = T_m^{Al} = 922.43$ K[36,42]) and a bulk pressure of 1 bar. Periodic boundary conditions were applied in all Cartesian directions. The production data were collected from constant volume, constant temperature (NVT) MD simulation runs at 922.43 K. The pressure of the system was monitored to ensure that the component of the pressure normal to the interface (p_z) remained at 1 bar. Under these conditions, the calculated equilibrium Al mole fractions in bulk liquid Pb and in bulk liquid Al are 0.0085(5) and 0.99988(3), respectively, indicating that the two liquids possess near mutual immiscibility. For these and all subsequent reported data, the values in parentheses represent 95% confidence intervals (calculated using block averages) in the last digits shown.

Because the broadening due to capillary-wave fluctuations is strongly dependent upon interfacial area, we have employed three simulation systems with different interfacial areas, hereafter labeled as A, B, and C. Each system has nearly equal parts Al(l) and Pb(l). The particle numbers and system sizes are summarized in Table 1. Figure 1a shows an NVT snapshot of the two equilibrated Al−Pb liquid−liquid interfaces for system A. In this figure, the two interfaces (upper and lower) in the simulation box are separated by ∼50 Å in the z direction. At this separation, we have verified that the interaction between the interfaces is negligible and that the liquid between the interfaces has properties identical to bulk Al (or Pb).

Also listed in Table 1 are liquid−liquid interfacial free energies γ_{ll} for this system at 922.43 K and 1 bar. These were

Table 1. MD Simulations of Al−Pb Liquid−Liquid Interface at 922.43K, System Sizes and Interfacial Free Energy Measured Using Eq 2[a]

ID	L_x, Å	L_y, Å	L_z, Å	N_{Al}	N_{Pb}	γ_{ll}^{KB}, mJ/m^2
A	80.5	81.3	181.3	32 256	17 851	253 (2)
B	246.4	36.9	100.0	25 386	13 267	252 (2)
C	739.2	36.9	130.5	96 768	53 553	252.4 (11)

[a]The values in parentheses represent 95% confidence level errors in the last digits shown.

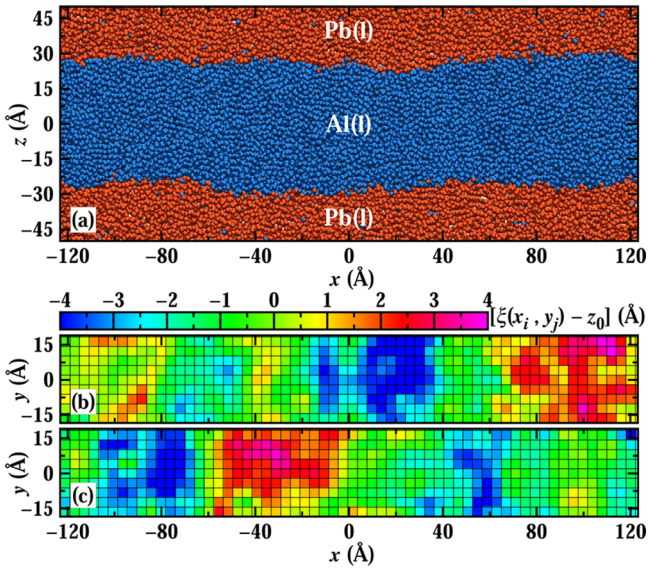

Figure 1. (a) Snapshot of equilibrated Al−Pb liquid−liquid interfaces for system C at 922.43K and 1 bar. (b) Coarse-grained plot of the instantaneous position, $\xi(x_i,y_j) - z_0$, for the upper interface, where z_0 is the position of the global GDS and the grid size, λ_{xy}, is 4.10 Å. (c) Same as part b for the lower interface.

calculated from the simulation data using the mechanical definition of interfacial free energy via the Kirkwood−Buff (KB) equation:[37]

$$\gamma_{ll}^{KB} = \int_{-\infty}^{\infty} [p_n(z) - p_t(z)]\, dz \tag{2}$$

where z is the direction normal to the interface and p_n and p_t are the normal and transverse components of the pressure tensor, respectively. The values for γ_{ll}^{KB} for the three different system sizes are equal within the statistical error.

For each equilibrated liquid−liquid interface, the mean interfacial total density and the individual Al and Pb density profiles [$\rho(z)$, $\rho_{Al}(z)$, and $\rho_{Pb}(z)$] were calculated by binning the simulation box in the z direction with bin size (Δz = 0.05 Å) and time-averaging the number of atoms over the xy plane in each discrete bin divided by the volume of the bin ($V_z = L_x L_y \Delta z$),

$$\rho(z) = \frac{\langle N_z \rangle}{V_z}, \quad \rho_{Al}(z) = \frac{\langle N_z^{Al} \rangle}{V_z}, \quad \rho_{Pb}(z) = \frac{\langle N_z^{Pb} \rangle}{V_z} \tag{3}$$

where $\langle N_z \rangle$, $\langle N_z^{Al} \rangle$ and $\langle N_z^{Pb} \rangle$ are the time average number of total, Al, and Pb atoms in the discrete bin, and z coordination was measured relative to a global Gibbs dividing surface (GDS), z_0, defined such that the global excess number of Al atoms is zero.[36,42]

dx.doi.org/10.1021/jp5019313 | J. Phys. Chem. B 2014, 118, 8373−8380

III. GRID-BASED INTERFACIAL CAPILLARY WAVE ANALYSIS

A. Determination of Interfacial Position. To resolve the capillary fluctuations and determine the intrinsic density profile within a molecular dynamics simulation, it is necessary to have a procedure to obtain precise instantaneous real-space interfacial configurations. A number of methods to do this have been proposed in the literature.[7−10,12,25,26,30,44] (See refs 12 and 30 for a recent comprehensive critical assessment.) Although most of these methods have been specifically developed for liquid−vapor interfaces, all are also applicable to the study of the intrinsic structure of the interface between two immiscible liquids, with various levels of accuracy and computational speed. The most accurate method is the intrinsic sampling method (ISM),[7] in which each instantaneous interfacial configuration is fitted with a self-consistent Fourier function, although this high precision method comes at considerable computational cost in comparison with other methods.

In this work, we employ the GIP method reported in refs 9 and 25. This method was chosen because its low computational cost allows for rapid calculation of interfacial position. There are, however, some limitations in accuracy that must be addressed by careful optimization of the method for the specific system, but these limitations have been reported to be less severe in simulations of atomic (as opposed to molecular) fluid interfaces.[30] In the GIP method, the simulation box is partitioned into $n_x \times n_y$ square prisms, with the plane parallel to the interface divided into a grid of squares. Each prism has size $\lambda_{xy} \times \lambda_{xy} \times L_z$, where $\lambda_{xy} = L_x/n_x = L_y/n_y$. In each prism, the position of the liquid−liquid interface for each grid point is defined as the arithmetic average of the z coordinates of the Al atom that protrudes furthest into the Pb liquid while still being connected to the Al bulk liquid and the corresponding Pb atom protruding into the Al fluid phase. The interfacial positions for all prisms are thus obtained as a coarse-grained grid mesh description of the instantaneous liquid−liquid interfacial configuration, $\xi(x_i,y_j)$, in which $x_i = i \times \lambda_{xy}$, $i = 1 \sim n_x$; $y_j = j \times \lambda_{xy}$, $j = 1 \sim n_y$. Because of periodic boundary conditions, there are two interfaces within a single simulation box. An example of this coarse graining is shown in Figure 1 using a grid size of 4.10 Å and showing both independent interface configurations.

As discussed in ref 30, the GIP method is capable of correctly determining the estimated shape of the instantaneous interface and the intrinsic density profile but requires selection of an optimal grid resolution (λ_{xy}) for the specific system. When the resolution is too low, the method fails to yield a qualitatively accurate description of the surface. However, if the resolution is too high, the number of atoms in each grid prisms becomes too small, making the determination of $\xi(x_i,y_j)$ difficult: for the higher resolutions, some prisms were found to contain no atomic centers, yielding an undefined value of $\xi(x_i,y_j)$. According to refs 12 and 30, the optimal grid size should correspond roughly to the largest atomic diameter in the system, which in our system is that of Pb. For comparison, we have examined grid sizes from 18.47 Å down to 3.08 Å, but most of the analysis was performed using λ_{xy} = 3.52 Å, which is slightly larger than the atomic diameter of Pb (3.22 Å), as measured by the position of the first peak in the bulk Pb radial distribution function (RDF), which is 3.22 Å at 922.43 K and 1 bar pressure. In addition, in this GIP analysis, we exclude Al atoms that are part of the Pb bulk fluid; the solubility of Al in Pb is about 1% at liquid−liquid coexistence.

B. Fluctuation Spectrum and Extraction of Interfacial Free Energy. According to classical CWT in which the macroscopic surface tension, γ_{ll}, is assumed to be independent of the wave vector ($\mathbf{q}$), the Hamiltonian for the system can be constructed from the work done in changing the surface area from a reference state (the time-averaged flat interface) to the instantaneous value, $\xi(\mathbf{r})$, with $\mathbf{r} = (x,y)$):

$$\mathcal{H}_{cw} = \gamma_{ll} \int [\sqrt{1 + |\nabla \xi(\mathbf{r})|^2} - 1]\, dr \tag{4}$$

where $\nabla = \hat{e}_x\, (\partial/\partial x) + \hat{e}_y\, (\partial/\partial y)$ and $\hat{e}_x$ and $\hat{e}_y$ are the unit vectors along the x and y directions. One can also write the interfacial position in its two-dimensional Fourier representation,

$$\xi(\mathbf{r}) = \sum_{\mathbf{q}\neq 0} \hat{\xi}_{\mathbf{q}} \exp(i\mathbf{q}\cdot\mathbf{r}) \tag{5}$$

in which the wave vector $\mathbf{q} = (q_x,q_y) = (2\pi m_x \hat{e}_x/L_x) + (2\pi m_y \hat{e}_y/L_y)$, with $m_x,m_y = 0, \pm 1, \pm 2, ..., \pm \infty$. Under conditions that the capillary fluctuations are weak, the Hamiltonian (eq 4) can be truncated to quadratic order in $|\hat{\xi}_{\mathbf{q}}|$ to give

$$\mathcal{H}_{cw} = \frac{1}{2}\gamma_{ll} L_x L_y \sum_{\mathbf{q}\neq 0} q^2 |\hat{\xi}_{\mathbf{q}}|^2 \tag{6}$$

in which case each fluctuation excitation mode becomes an independent harmonic oscillator. With this approximation, application of the equipartition theorem (which states that each quadratic excitation mode contributes $k_B T$ to the energy) yields

$$\langle |\hat{\xi}_{\mathbf{q}}|^2 \rangle = \frac{k_B T}{L_x L_y \gamma_{ll} q^2} \tag{7}$$

in which $q = (q_x^2 + q_y^2)^{1/2}$ and k_B is the Boltzmann constant. There is an upper limit cutoff to the wave-vector magnitude, $q_c = 2\pi/\lambda_c$, where λ_c is a lower distance cutoff on the order of the molecular (or atomic) size, below which the classical CWT and eq 7 is applicable. Below this length scale, the nonclassical capillary wave fluctuation contribution to the total interfacial tension will yield deviations from the macroscopic surface tension.[45−47] In addition, in a finite computer simulation, there is also a lower bound on the magnitude of the wave vector, q_{min}, corresponding to wavelengths on the order of the system size.

In this work, we use the GIP method to calculate the interfacial position $\xi(x_i,y_j)$ for the Al−Pb liquid−liquid interface at coexistence. From this data, we confirm the validity of CWT for this system through an comparison of the calculated Fourier spectrum of ξ with the CWT prediction from eq 7. We determine the liquid−liquid interfacial free energy estimate from this method, γ_{ll}^{cfm} (CFM = capillary fluctuation method) by fitting the low-q spectrum of ξ using weighted linear least-squares on a log−log plot of ξ versus q. The CFM estimate of γ_{ll}^{cfm} is compared with that calculated using the Kirkwood−Buff equation (eq 2).

C. Probability Distribution of Interfacial Position. The probability distribution of the interfacial position, $P_\xi(z)$, is necessary for evaluating the validity of the convolution assumption (eq 1). Generally, this quantity is calculated within classical CWT assuming that the Fourier components $\hat{\xi}_{\mathbf{q}}$ in eq 7 are independent Gaussian random variables in the range $q_{min} < |\mathbf{q}| < q_c$ (eq 6). Within the CWT approximation, the real-space

dx.doi.org/10.1021/jp5019313 | J. Phys. Chem. B 2014, 118, 8373−8380

probability distribution of the instantaneous interfacial position is also Gaussian distributed,

$$P_{\xi}(z) = \frac{1}{\Delta_{\xi,\mathrm{CWT}}\sqrt{2\pi}} \exp\left(-\frac{(z-z_0)^2}{2{\Delta_{\xi,\mathrm{CWT}}}^2}\right) \tag{8}$$

in which the interfacial roughness is measured by the Gaussian variance, ${\Delta_{\xi,\mathrm{CWT}}}^2$ (the capillary fluctuation mean-square amplitude), which is equal to the sum of the uncorrelated probabilities for the Fourier components with mean-square values $|\hat{\xi}_{\mathbf{q}}|^2$ for any q between the lower and the upper wave vector limits ($q_{\min}$ and q_c),

$${\Delta_{\xi,\mathrm{CWT}}}^2 = \sum_{\mathbf{q}\neq 0} \langle |\hat{\xi}_{\mathbf{q}}|^2 \rangle \tag{9}$$

In this work, instead of using the CWT approximation for $P_{\xi}(z)$, we calculate this probability distribution *directly* from the MD simulation using the discretized interfacial position $\xi(x_i,y_j)$ calculated using the GIP method. In terms of $\xi(x_i,y_j)$, the probability distribution, $P_{\xi}^{\mathrm{MD}}(z)$, is given by[48]

$$P_{\xi}^{\mathrm{MD}}(z) = \frac{1}{L_x L_y}\int_0^{L_x}\int_0^{L_y} \delta[\xi(x,y) - z]\,\mathrm{d}x\,\mathrm{d}y \tag{10}$$

To better automate the numerical integration of eq 10, we approximate the delta function in the formula as a Gaussian function with a small variance. We have verified that using a Gaussian function with a variance in the range 10^{-8}–10^{-6} Å^2 does not affect the resulting probability distribution significantly. In our analysis, we also investigate the effect of the grid size on this direct calculation of $P_{\xi}^{\mathrm{MD}}(z)$.

D. Intrinsic Interfacial Structure. From the instantaneous interfacial position $\xi(x,y)$, the intrinsic density profile of the liquid–liquid interface can be defined as follows:[7]

$$\hat{\rho}(z) = \left\langle \frac{1}{n_x n_y}\sum_{i}^{n_x}\sum_{j}^{n_y} \tilde{\rho}(z - \xi(x_i,y_j)) \right\rangle \tag{11}$$

where $\tilde{\rho}(z)$ is the instantaneous number density as a function of the coordinate normal to the interface (z). In the simulations, $\tilde{\rho}(z - \xi(x_i,y_j))$ is calculated by subdividing the GIP prism (x_i,y_j) into n_z bins along the z axis and calculating the number of particles in each z bin and dividing by the bin volume. In principle, the intrinsic structure is independent of system size, the magnitude of fluctuation, and details of the computational method. So intrinsic structures are determined for all systems and grid sizes employed in this study to assess the precision of our results.

Because we have calculated $P_{\xi}^{\mathrm{MD}}(z)$, $\rho(z)$, and $\hat{\rho}(z)$ independently in this work, we are able to assess directly the validity of the convolution assumption (eq 1) for the liquid–liquid interface under study. Recent work using the ISM method on liquid–vapor interfaces[35] has concluded that the measured mean density profile exhibits significant variation from that predicted using the convolution approximation. To examine the convolution approximation for our system, it is useful to define reduced density profiles (following Sides et al.,[48]) which vary across the interface from −1 to 1:

$$\Psi(z) = \frac{2}{\rho_{\mathrm{Al}}^{\mathrm{l}} - \rho_{\mathrm{Pb}}^{\mathrm{l}}}\left[\rho(z) - \frac{\rho_{\mathrm{Al}}^{\mathrm{l}} + \rho_{\mathrm{Pb}}^{\mathrm{l}}}{2}\right] \tag{12}$$

$$\psi(z) = \frac{2}{\rho_{\mathrm{Al}}^{\mathrm{l}} - \rho_{\mathrm{Pb}}^{\mathrm{l}}}\left[\hat{\rho}(z) - \frac{\rho_{\mathrm{Al}}^{\mathrm{l}} + \rho_{\mathrm{Pb}}^{\mathrm{l}}}{2}\right] \tag{13}$$

Here, $\Psi(z)$ and $\psi(z)$ are the reduced mean and intrinsic density profiles, respectively.

To assess the validity of the convolution approximation directly, using eq 13, we calculate the reduced mean density profile, $\Psi_{\mathrm{conv}}(z)$, as a convolution of the independently calculated intrinsic density profile and the probability distribution of the interfacial position, $P_{\xi}^{\mathrm{MD}}(z)$. After introducing the order parameter interfacial profiles, the convolution eq 1 becomes

$$\Psi_{\mathrm{conv}}(z) = \int \mathrm{d}z'\,\psi(z - z')\,P_{\xi}(z') \tag{14}$$

The reduced mean density calculated from direct convolution, $\Psi_{\mathrm{conv}}(z)$, will be compared with the independently calculated reduced mean interfacial total density profile $\Psi(z)$ in assessing the validity of eq 1 for this system.

Another route to the intrinsic density profile, following Sides et al.,[48] is to assume that the underlying probability distributions generating $\Psi(z)$ and $\psi(z)$ are Gaussian. Within this approximation, the convolution equation (eq 1) can be expressed as a relation between the variances of the underlying probability distributions

$$\Delta^2 = {\Delta_{\xi}}^2 + {\Delta_0}^2 \tag{15}$$

where ${\Delta_{\xi}}^2$ is the variance of the interfacial position distribution $P_{\xi}^{\mathrm{MD}}(z)$, and Δ^2 and ${\Delta_0}^2$ are the variances of the probability distributions for the reduced mean and intrinsic density profiles ($\Psi'(z)$ and $\psi'(z)$, respectively). The assumption of Gaussian form for $\Psi'(z)$ and $\psi'(z)$ implies an error-function form ($f(z) = \mathrm{erf}(\pi z/w)$) for both $\Psi(z)$ and $\psi(z)$. Sides et al.[48] have shown for LJ vapor–liquid interfaces that the error function form better describes the mean density profile than does the often-used hyperbolic tangent profile. In this work, ${\Delta_{\xi}}^2$ is determined directly from the variance of the measured interfacial position probability, $P_{\xi}^{\mathrm{MD}}(z)$ (eq 10), which is well approximated by a Gaussian function. Combining eqs 15 and 13, we can determine ${\Delta_0}^2$ and construct an "intrinsic profile", $\psi_{\mathrm{erf}}(z)$, using the error-function form:

$$\psi_{\mathrm{erf}}(z) = \mathrm{erf}\left(\frac{\pi z}{\sqrt{2\pi(\Delta^2 - {\Delta_{\xi}}^2)}}\right) \tag{16}$$

This $\psi_{\mathrm{erf}}(z)$ will be compared with the $\psi(z)$ determined from the grid-based method.

IV. RESULTS AND DISCUSSION

A. Interfacial Free Energy and Fluctuation Spectrum. As outlined in Section 3.2, we have calculated the liquid–liquid interfacial fluctuation spectrum for each of the three system sizes listed in Table 1 using the interfacial positions determined using the GIP method. For each of these calculations, GIP grid sizes (λ_{xy}) ranging from 2.46 to 18.47 Å were used. The spectra for the largest system (system C) with two different grid sizes (3.08 and 5.28 Å) are shown in the top panel of Figure 2, and the bottom panel compares the fluctuation spectrum for different systems (A and C) with the same grid size, λ_{xy} = 4.1 Å. In both panels of Figure 2, the CWT prediction is plotted as a reference line. In Figure 2, the amplitude of the fluctuation

dx.doi.org/10.1021/jp5019313 | J. Phys. Chem. B 2014, 118, 8373–8380

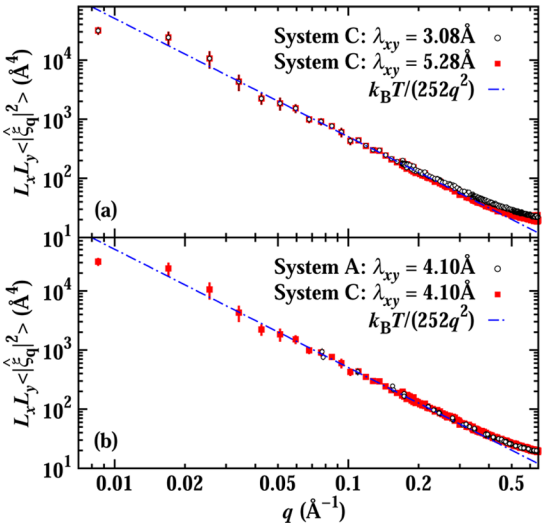

Figure 2. Capillary fluctuation spectra of liquid−liquid Al−Pb interfaces. (a) Comparison for system C using two different grid sizes. (b) Comparison of systems A and C using fixed grid size. CWT predictions are plotted with reference to dashed−dotted lines.

spectrum is scaled by the interfacial area to facilitate direct comparison between different system sizes. For q in the range $q_l \approx 2\pi/L_x < q < \sim 0.4$, the q^{-2} dependence predicted by the CWT is well reproduced.

Using weighted least-squares regression, we fit $\ln(\xi_q)$ versus $\ln(q)$ in the range $q_l < q < 0.17$ to obtain γ_{ll}^{cfm} using eq 7. The results for all systems (and grid sizes) studied are summarized in Table 2. These results for γ_{ll}^{cfm} (252 mJ m^{-2}) are in excellent

Table 2. Results from MD Simulation Analysis of Capillary Fluctuations of a Coexisting Al−Pb Liquid−Liquid Interface at 922.43 K and 1 Bar[s]

ID	λ_{xy}, Å	Δ^2, Å^2	Δ_ξ^2, Å^2	Δ_0^2, Å^2	γ_{ll}^{cfm}, mJ m^{-2}
A	4.10	5.16 (5)	2.66 (7)	2.50 (8)	250 (5)
B	4.10	6.65 (18)	3.9 (2)	2.8 (3)	252 (6)
C	3.08	10.6 (4)	8.8 (6)	1.8 (7)	252 (4)
C	3.52	10.6 (4)	8.2 (6)	2.4 (7)	252 (3)
C	4.10	10.6 (4)	7.8 (6)	2.8 (7)	252 (3)
C	4.62	10.6 (4)	7.6 (6)	3.0 (7)	253 (4)
C	5.28	10.6 (4)	7.4 (6)	3.2 (7)	252 (3)
C	7.39	10.6 (4)	7.0 (6)	3.6 (7)	254 (6)
C	18.47	10.6 (4)	6.1 (6)	4.5 (8)	252 (17)

[s]Data is shown for three different system sizes (A, B, and C) (see Table 1) and varying GIP grid size, λ_{xy}. Shown are the variances (widths) corresponding to the mean density profile, Δ^2; interfacial position distribution, Δ_ξ^2; and the intrinsic density profile, Δ_0^2. Also shown are the interfacial free energies measured from the capillary fluctuation spectrum, γ_{ll}^{cfm}. Numbers in parentheses are 95% confidence errors for the last digits shown.

agreement with those calculated mechanically using the Kirkwood−Buff equation (eq 2, which are listed in Table 1. In addition, the statistical precision of the CFM results is similar to the KB calculated values. The agreement between the interfacial free energy calculation within the CFM with that using a mechanical approach confirms the validity of the CFM predictions with respect to interfacial thermodynamics and the relative insensitivity of this result to the system and grid sizes. The mechanical and CFM estimates of the liquid−liquid interfacial free energy, although in good agreement with each other, are significantly larger (about a factor of 2) for this model than that reported in a previous experimental study for this system (125.5 mJ m^{-2}).[49]

B. Direct Calculation of the Probability Distribution for Interfacial Position. Using the method outlined in Section 3.4, we have directly calculated the probability distribution function for the interfacial position from the calculated fluctuation spectra for all systems and grid sizes studied here. In the top panel of Figure 3, we show the directly

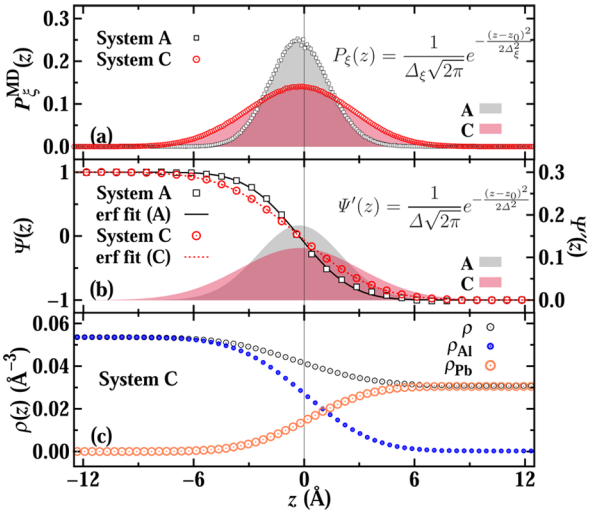

Figure 3. (a) Calculated fluctuation probability distribution $P_\xi^{MD}(z)$ for system A (open squares) and C (solid circles) using the GIP method (grid size λ_{xy} = 4.10 Å). Also shown are the Gaussian fits of these distributions (shaded areas). (b) Reduced mean-density profiles $\Psi(z)$ for the same systems are in part a and fitted with error functions (solid and dotted lines). The underlying Gaussian forms for $\Psi'(z)$ are shown as shaded areas. (c) Mean density profiles for Al (blue circles) and Pb (orange circles). Also shown is the total mean density (black circles).

calculated distribution $P_\xi^{MD}(z)$ for systems A and C using a fixed grid size of 4.10 Å. These two distributions (for A and C) are well fit by Gaussian functions (also shown in Figure 3. The calculated variances, Δ_ξ^2, of $P_\xi^{MD}(z)$ for each system studied are listed in Table 2. As expected, system C has a larger width fluctuation distribution than systems A and B because of the larger interfacial cross section area.

C. Mean Density Profiles. The reduced mean density profiles (all atom) determined from the MD simulation for systems A and C (grid size 4.10 Å) are shown in the middle panel of Figure 3. In agreement with Sides et al.,[48] the mean density profiles are well fit by error function profiles, also shown in Figure 3 (middle panel). The interfacial width for the mean density profiles, as measured by the variance, Δ^2, of underlying probability function $\Psi'(z)$ (which is well described by a Gaussian function), has been calculated for all system sizes studied (see Table 2), and the fits for systems A and C (grid size 4.10 Å) are included in the middle panel of Figure 3. As expected, the mean interfacial width increases with increasing system size, as a result of capillary fluctuations. In the bottom panel of Figure 3 are the separate individual density profiles for Al and Pb. The overlap of these density profiles is due to the capillary fluctuations and does not imply mixing of Al and Pb in the interfacial region; this will be shown clearly in the intrinsic profiles.

dx.doi.org/10.1021/jp5019313 | J. Phys. Chem. B 2014, 118, 8373−8380

D. Intrinsic Density Profiles. As discussed in Section 3.4, a qualitative estimate of the width of the intrinsic interfacial profile can be determined from the mean density profile width, Δ, and that of the interfacial position distribution, Δ_ξ, using eq 15. For the systems studied, the results of this calculation are listed in Table 2. The corresponding error function form of the intrinsic density profiles (eq 16) for systems A and C (grid size 4.10 Å) is shown in Figure 3. Except for the extremal grid sizes (very smallest or largest), the intrinsic interfacial widths for the three different system sizes (A, B, and C) are equal within the error bars of the calculations, consistent with the assumption that these represent intrinsic profiles unbroadened by capillary fluctuations. Because of the assumption of error-function form, the intrinsic profiles so calculated represent only a qualitative picture of the true intrinsic profile because they exclude the possibility of oscillatory intrinsic structure.

As noted earlier, classical DFT studies of LLIs[50,51] predict structural oscillations on either side of the LLI, similar to those predicted at liquid–vapor interfaces.[33] These oscillations represent density response of the fluids to the presence of the inhomogeneity (interface) and are, thus, related to the radial density functions of the bulk fluids. To better resolve the intrinsic interfacial profile for the Al–Pb liquid–liquid interface, we have directly calculated the intrinsic density profiles $\hat{\rho}(z)$ from our MD simulation results using the GIP analysis and eq 11, as outlined in Section 3.4. The reduced intrinsic total density profile, $\psi(z)$, corresponding to system size C and using a grid size of 3.52 Å is shown in the top panel of Figure 4. In the bottom panel of Figure 4, we show the intrinsic profiles of the individual components, Al and Pb, scaled relative to the respective bulk density values. As predicted, the intrinsic density profiles for this system show significant oscillations away from the interfacial plane. Unlike the results of Geysermans and Ponkis,[32] who examined the LLI of symmetric LJ model, the intrinsic density profile for the Al–Pb LLI studied here shows significant asymmetry due to the differences in size and interaction of Al and Pb.

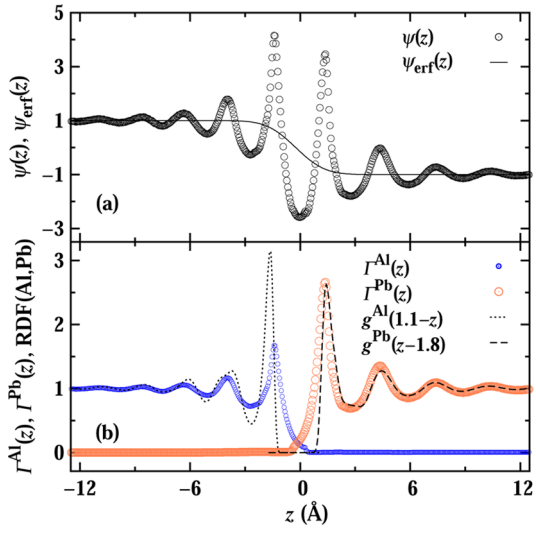

Figure 4. (a) Intrinsic density profile determined with the grid-based method (λ_{xy} = 4.10 Å) for C, shown with rescaled magnitude ($\psi(z)$) and with open symbols, compared with deconvoluted density profile ($\psi_{\mathrm{erf}}(z)$). (b) Intrinsic Al (smaller open circles) and Pb (larger open circles) density rescaled with their bulk liquid density, $\Gamma^{\mathrm{Al}}(z) = \hat{\rho}_{\mathrm{Al}}(z)/\rho_{\mathrm{Al}}^{\mathrm{bulk}}$, $\Gamma^{\mathrm{Pb}}(z) = \hat{\rho}_{\mathrm{Pb}}(z)/\rho_{\mathrm{Pb}}^{\mathrm{bulk}}$, compared with bulk liquid radial distribution functions, RDF, represented with dotted and dashed lines and aligned together to fit the tail peaks with the rescaled intrinsic densities, respectively.

To examine the relationship of these oscillations in the intrinsic density profiles to the bulk liquid structure, we also show the radial distribution functions, $g(r)$, for pure liquid Al and Pb in the lower panel of Figure 4. For comparison, these RDF's are shifted to be in register with the intrinsic density profiles at large distances. In this figure, the intrinsic density profile for Pb is nearly identical to the bulk liquid Pb RDF. Although the position of the first peak of the intrinsic density for Al is slightly displaced relative to the first peak of the RDF and the magnitude is somewhat reduced, the agreement at long distances is good.

E. Test of Convolution Assumption. Because we have calculated the mean density profile, $\rho(z)$; the interfacial position probability distribution, $P_\xi(z)$; and the intrinsic density profile, $\hat{\rho}(z)$, independently and directly from the MD trajectories, we can directly test the convolution approximation (eq 1) by convoluting $P_\xi(z)$ with $\hat{\rho}(z)$ and comparing the result with the actual mean density profile measured in the simulation. The result of this comparison for system C with a grid size of 3.52 Å is shown in Figure 5 (top panel). In this figure, the directly calculated reduced mean density profile, $\Psi(z)$, is shown to be in near-perfect agreement with that determined from the convolution of $P_\xi(z)$ and the reduced intrinsic profile, $\psi(z)$, using eq 14, showing that for this system, the convolution assumption (eq 1) is valid. In addition, the validity of the convolution assumption is independent of system grid size (Figure 5, bottom panel).

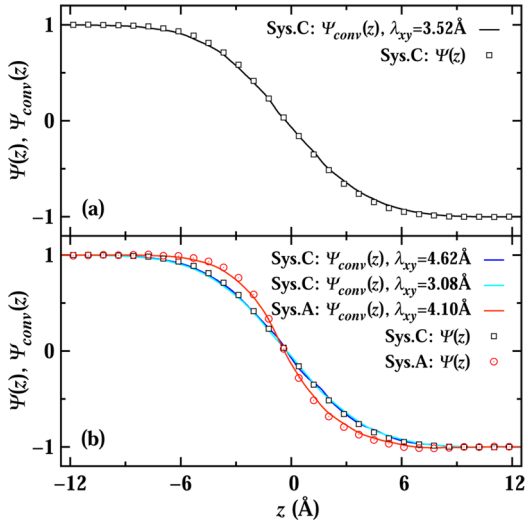

Figure 5. Top panel: Mean density profile (open squares) compared with convolution of the grid-based intrinsic density profiles and the calculated $P_\xi^{\mathrm{MD}}(z)$ (solid line) for system C with the optimal grid size (3.52 Å). Bottom panel: Same as top panel, except for system C at additional values of λ_{xy}, to show the grid size dependence, and for the smaller system A.

This result differs from recent results by Fernandez et al. using the ISM on an LJ liquid–vapor interface.[35] In this study, the mean density profile produced by the convolution of the measured intrinsic density profile and the probability of interfacial position is shown to deviate quantitatively from the measured mean density profile. In this ISM study, it is argued that at the high resolution of the ISM ($q_c \approx 2\pi/\sigma$, σ is the LJ

dx.doi.org/10.1021/jp5019313 | J. Phys. Chem. B 2014, 118, 8373–8380

diameter of the atom/molecule), the convolution assumption breaks down as a result of the emergence of non-neglectible correlation between fluctuations in the interfacial shape and in the intrinsic structure.

There are a number of potential factors that could account for the qualitatively different conclusions between our current LLI study and the ISM liquid–vapor study in ref 35. First, the ISM is a higher-precision method than the GIP used here. However, for atomic systems with a grid size on the order of the largest atomic diameter, GIP has been shown to give results consistent with the more detailed ISM analysis.[12] In addition, we have checked the validity of the convolution approximation for a number of grid sizes from 4.5 down to 3.08 Å and found quantitative agreement between the measured mean density profile and that produced by convolution in all cases. The second possible explanation for the difference stems from the fact that in our current study, we use the directly calculated probability distribution, $P_\xi^{MD}(z)$, in the convolution, whereas Fernandez et al.[35] employ the Gaussian CWT prediction for $P_\xi(z)$ using a microscopic cutoff predicted by the ISM (presumably, that corresponding to the atomic diameter). In determining $P_\xi^{MD}(z)$, we make no assumptions as to its functional form (although it is well fit by a Gaussian) nor as to the microscopic cutoff used. Therefore, deviation from eq 1 seen in the ISM study may have more to do with the assumptions as to the form of $P_\xi(z)$ than with the validity of eq 1 itself. Finally, in this study, we examine a liquid–liquid interface, whereas ref 35 examines a liquid–vapor interface. It is possible that there is a fundamental difference between these two types of interfaces with respect to the validity of eq 1, which would be an issue requiring further study.

V. SUMMARY

Using MD simulation, we have carried out a series of simulations to study in detail the structure and thermodynamics of the Al/Pb liquid–liquid interface at 922.43 K and 1 bar using an EAM model due to Landa et al.[41] Most such studies on liquid–liquid interfaces (LLI) involve either molecular systems (such as hydrocarbons and water) or highly idealized atomic models, such as a symmetric Lennard-Jones system, and the purpose of the current work is to examine a LLI of two immiscible atomic fluids, using realistic potentials. In our analysis, the instantaneous interfacial position was determined using the grid-based intrinsic profile method.[9,25] This method, although less precise than the higher-resolution intrinsic sampling method,[7] has been shown to give accurate results for atomic systems for grid sizes on the order of the largest atom (in this case, Pb). The liquid–liquid interfacial free energy, γ_{ll}, for this system was calculated using both a mechanical approach using the Kirkwood–Buff equation (eq 2 and the capillary fluctuation method,[40] which examines the power spectrum of fluctuations in the interfacial spectrum. Both methods give consistent results, with γ_{ll} = 252 mJ m^{-2} for this model, which is approximately twice the reported experimental value for this system at this temperature.[49]

In addition to the thermodynamics, we use the GIP analysis to obtain a detailed description of the structure of the Al–Pb liquid–liquid interface by directly and independently determining both the mean and intrinsic density profiles, $\rho(z)$ and $\hat{\rho}(z)$, as well as the probability distribution of interfacial position, $P_\xi^{MD}(z)$. In this work, the probability distribution, $P_\xi^{MD}(z)$, is calculated directly from the simulation using the GIP analysis, as opposed to using the capillary wave theory prediction (eq 8), which requires the specification of a lower wavelength limit on capillary fluctuations. Like previous studies on liquid–liquid and liquid–vapor interfaces, the intrinsic density profile for the Al–Pb LLI shows pronounced oscillations near the interfacial plane. Consistent with classical DFT predictions, these oscillations are quantitatively similar to the radial distributions functions for the bulk liquid phases. In addition, we show that the usual convolution assumption (eq 1) that the mean density profile, $\rho(z)$, can be represented by a convolution of the intrinsic density profile, $\hat{\rho}(z)$, and the probability distribution, $P_\xi^{MD}(z)$, is quantitatively valid for this system and that its validity is independent of the grid size used in the GIP analysis.

Note that at the temperature of this study (922.43 K, the melting temperature of Al for this model), Al and Pb exhibit nearly complete mutual immiscibility in their liquid phases, which greatly simplifies the determination of the interfacial position. Extending this study to higher temperatures where the miscibility gap narrows for this system would require significant modification of the method used to determine the interfacial position for miscible liquid–liquid interfaces.

AUTHOR INFORMATION

Corresponding Author

*E-mail: blaird@ku.edu.

Notes

The authors declare no competing financial interest.

ACKNOWLEDGMENTS

Y.Y. and B.B.L. acknowledge funding from the National Science Foundation under Grant CHE-0957102. The authors thank Prof. Mark Asta, Dr. David Olmsted, and Dr. Tim Frolov for helpful discussions.

REFERENCES

(1) Reymond, R.; Fermin, D.; Lee, H.; Girault, H. Electrochemistry at liquid/liquid interfaces: methodology and potential applications. *Electrochem. Acta* **2000**, *45*, 2647–2662.

(2) Arrigan, D. Voltametry of proteins at liquid–liquid interfaces. *Ann. Rep. Prog. Chem. C* **2013**, *109*, 167.

(3) Gelbart, W.; Ben-Shaul, A.; Roux, D., Eds. *Micelles, membranes, microemulsions, and monolayers*; Springer-Verlag: New York, 2003.

(4) Lin, Y.; Skaff, H.; Emrick, T.; Dinsmore, A.; Russell, T. Nanoparticle assembly and transport at liquid–liquid interfaces. *Science* **2003**, *299*, 226–229.

(5) Rowlinson, J.; Widom, B. *Molecular Theory of Capillarity*; Dover books on chemistry; Dover Publications: Mineola, NY, 2002.

(6) Buff, F. P.; Lovett, R. A.; Stillinger, F. H. Interfacial density profile for fluids in the critical region. *Phys. Rev. Lett.* **1965**, *15*, 621–623.

(7) Chacón, E.; Tarazona, P. Intrinsic profiles beyond the capillary wave theory: A Monte Carlo study. *Phys. Rev. Lett.* **2003**, *91*, 166103.

(8) Chowdhary, J.; Ladanyi, B. Water-hydrocarbon interfaces: effect of hydrocarbon branching on interfacial structure. *J. Phys. Chem. B* **2006**, *110*, 15442–15453.

(9) Jorge, M.; Cordeiro, M. Intrinsic Structure and Dynamics of the Water/Nitrobenzene Interface. *J. Phys. Chem. C* **2007**, *111*, 17612–17626.

(10) Pátray, L. B.; Hantal, G.; Jedlovszky, P.; Vincze, A.; Horvai, G. A new method for determining the interfacial molecules and characterizing the surface roughness in computer simulations: Application to the liquid–vapor interface of water. *J. Comput. Chem.* **2008**, *29*, 945–956.

(11) Willard, A.; Chandler, D. Instantaneous liquid interfaces. *J. Phys. Chem. B* **2010**, *114*, 1954–1958.

(12) Jorge, M.; Jedlovszky, P.; Cordeiro, M. A critical assessment of methods for the intrinsic analysis of liquid lnterfaces: 1. Surface site distributions. *J. Phys. Chem. C* **2010**, *114*, 11169−11179.
(13) Sega, M.; Kantorovich, S. S.; Jedlovszky, P.; Jorge, M. The generalized identification of truly interfacial molecules (ITIM) algorithm for nonplanar interfaces. *J. Chem. Phys.* **2013**, *138*, 044110.
(14) Tarazona, P.; Chacón, E. Monte Carlo intrinsic surfaces and density profiles for liquid surfaces. *Phys. Rev. B* **2004**, *70*, 235407.
(15) Chacón, E.; Tarazona, P.; Alejandre, J. The intrinsic structure of the water surface. *J. Chem. Phys.* **2006**, *125*, 014709.
(16) Pártay, L. B.; Jedlovszky, P.; Horvai, G. Structure of the liquid−vapor interface of water−acetonitrile mixtures as seen from molecular-dynamics simulations and identification of truly interfacial molecules analysis. *J. Phys. Chem. C* **2009**, *113*, 18173−18183.
(17) Darvas, M.; Pojják, K.; Horvai, G.; Jedlovszky, P. Molecular dynamics simulation and identification of the truly interfacial molecules (ITIM) analysis of the liquid-vapor interface of dimethyl sulfoxide. *J. Chem. Phys.* **2010**, *132*, 134701.
(18) Hantal, G.; Cordeiro, M. S.; Jorge, M. What does an ionic liquid surface really look like? Unprecedented details from molecular simulations. *Phys. Chem. Chem. Phys.* **2011**, *13*, 21230−21232.
(19) Hantal, G.; Voroshylova, I.; Cordeiro, M. S.; Jorge, M. A systematic molecular simulation study of ionic liquid surfaces using intrinsic analysis methods. *Phys. Chem. Chem. Phys.* **2012**, *14*, 5200−5213.
(20) Martinez, H.; Chacón, E.; Tarazona, P.; Bresme, F. The intrinsic interfacial structure of ionic surfactant monolayers at water−oil and water−vapour interfaces. *Proc. R. Soc. A* **2011**, *467*, 1939−1958.
(21) Tarazona, P.; Chacón, E.; Bresme, F. Intrinsic profiles and the structure of liquid surfaces. *J. Phys.: Condens Matter* **2012**, *24*, 284123.
(22) Bresme, F.; Chacón, E.; Tarazona, P.; Wynveen, A. The structure of ionic aqueous solutions at interfaces: An intrinsic structure analysis. *J. Chem. Phys.* **2012**, *137*, 114706.
(23) Bresme, F.; Chacón, E.; Tarazona, P.; Tay, K. Intrinsic structure of hydrophobic surfaces: The oil−water interface. *Phys. Rev. Lett.* **2008**, *101*, 056102.
(24) Bresme, F.; Chacón, E.; Tarazona, P. Molecular-dynamics investigation of the intrinsic structure of water−fluid interfaces via the intrinsic sampling method. *Phys. Chem. Chem. Phys.* **2008**, *10*, 4704−4715.
(25) Jorge, M.; Cordeiro, M. N. D. S. Molecular-dynamics study of the interface between water and 2-nitrophenyl octyl ether. *J. Phys. Chem. B* **2008**, *112*, 2415−2429.
(26) Pártay, L. B.; Horvai, G.; Jedlovszky, P. Molecular level structure of the liquid/liquid interface. Molecular-dynamics simulation and ITIM analysis of the water−CCl_4 system. *Phys. Chem. Chem. Phys.* **2008**, *10*, 4754−4764.
(27) Hantal, G.; Terleczky, P.; Horvai, G.; Nyulászi, L.; Jedlovszky, P. Molecular-level properties of the water-dichloromethane liquid/liquid interface, as seen from molecular-dynamics simulation and identification of truly interfacial molecules analysis. *J. Phys. Chem. C* **2009**, *113*, 19263−19276.
(28) Hantal, G.; Darvas, M.; Pártay, L.; Horvai, G.; Jedlovszky, P. Molecular level properties of the free water surface and different organic liquid/water interfaces, as seen from ITIM analysis of computer simulation results. *J. Phys.: Condens. Matter* **2010**, *22*, 284112.
(29) Pártay, L. B.; Horvai, G.; Jedlovszky, P. Temperature and pressure dependence of the properties of the liquid−liquid interface. A computer simulation and identification of the truly interfacial molecules investigation of the water−benzene system. *J. Phys. Chem. C* **2010**, *114*, 21681−21693.
(30) Jorge, M.; Hantal, G.; Jedlovszky, P.; Cordeiro, M. A critical assessment of methods for the intrinsic analysis of liquid interfaces: 2. Density profiles. *J. Phys. Chem. C* **2010**, *114*, 18656−18663.
(31) Bresme, F.; Chacón, E.; Tarazona, P. Force-field dependence on the interfacial structure of oil−water interfaces. *Mol. Phys.* **2010**, *108*, 1887−1898.
(32) Geysermans, P.; Pontikis, V. Interfacial layering and capillary roughness in immiscible liquids. *J. Chem. Phys.* **2010**, *133*, 074706.
(33) Evans, R.; Henderson, J.; Hoyle, D.; Parry, A.; Sabeur, Z. Asymptotic decay of liquid structure: oscillatory liquid-vapor density profiles and the Fisher−Widom line. *Mol. Phys.* **1993**, *80*, 755−775.
(34) Croxton, C.; Percus, J. R. *Fluid interfacial phenomena*; John Wiley: New York, 1986.
(35) Fernández, E. M.; Chacón, E.; Tarazona, P.; Parry, A. O.; Rascón, C. Intrinsic fluid interfaces and nonlocality. *Phys. Rev. Lett.* **2013**, *111*, 096104.
(36) Yang, Y.; Asta, M.; Laird, B. Solid-liquid interfacial premelting. *Phys. Rev. Lett.* **2013**, *110*, 096102.
(37) Kirkwood, J.; Buff, F. The statistical mechanical theory of surface tension. *J. Chem. Phys.* **1949**, *17*, 338−343.
(38) Nijmeijer, M. J. P.; Bakker, A. F.; Bruin, C.; Sikkenk, J. H. A molecular-dynamics simulation of the Lennard-Jones liquid−vapor interface. *J. Chem. Phys.* **1988**, *89*, 3789−3792.
(39) Hill, T. *An Introduction to Statistical Thermodynamics*; Dover Publications: Mineola, NY, 1960.
(40) Hoyt, J. J.; Asta, M.; Karma, A. Method for computing the anisotropy of the solid−liquid interfacial free energy. *Phys. Rev. Lett.* **2001**, *86*, 5530−5533.
(41) Landa, A.; Wynblatt, P.; Siegel, D.; Adams, J.; Mryasov, O.; Liu, X.-Y. Development of glue-type potentials for the Al−Pb system: phase diagram calculation. *Acta Mater.* **2000**, *48*, 1753−1761.
(42) Yang, Y.; Olmsted, D. L.; Asta, M.; Laird, B. B. Atomistic characterization of the chemically heterogeneous Al−Pb solid−lquid interface. *Acta Mater.* **2012**, *60*, 4960−4971.
(43) Plimpton, S. Fast parallel algorithms for short-range molecular dynamics. *J. Comput. Phys.* **1995**, *117*, 1−19.
(44) Pandit, S.; Bostick, D.; Berkowitz, M. L. An algorithm to describe molecular scale rugged surfaces and its application to the study of a water/lipid bilayer interface. *J. Chem. Phys.* **2003**, *119*, 2199−2205.
(45) Kayser, R. F. Effect of capillary waves on surface tension. *Phys. Rev. A* **1986**, *33*, 1948−1956.
(46) Weeks, J. D.; Van Saarloos, W. Implications of the Triezenberg−Zwanzig surface tension formula for models of interface structure. *J. Phys. Chem.* **1989**, *93*, 6969−6975.
(47) Chowdhary, J.; Ladanyi, B. Surface fluctuations at the liquid−liquid interface. *Phys. Rev. E* **2008**, *77*, 031609.
(48) Sides, S.; Grest, G.; Lacasse, M. D. Capillary waves at liquid−vapor interfaces: A molecular-dynamics simulation. *Phys. Rev. E* **1999**, *60*, 6708−6713.
(49) Hoyer, W.; Kaban, I.; Merkwitz, M. Liquid−liquid interfacial tension in immiscible binary Al-based alloys. *J. Opt. Adv. Mater.* **2003**, *5*, 1069.
(50) Napari, I.; Laaksonen, A.; Talanquer, V.; Oxtoby, D. A density functional study of liquid−liquid interfaces in partially miscible systems. *J. Chem. Phys.* **1999**, *110*, 5906−5912.
(51) Geysermans, P.; Elyeznasni, N.; Russier, V. Layered interfaces between immiscible liquids studied by density-functional theory and molecular-dynamics simulations. *J. Chem. Phys.* **2005**, *123*, 204711.